Supporting information on:

The reduced cohesion of homoconfigurational 1,2-diols

Beppo Hartwig[a], Manuel Lange[a], Anja Poblotzki[a], Robert Medel[a], Anne Zehnacker[b], Martin A. Suhm[a]*

a Institut für Physikalische Chemie, Georg-August-Universität Göttingen, Tammannstr. 6, 37077 Göttingen, Germany. E-mail: msuhm@gwdg.de

b Institut des Sciences Moléculaires d'Orsay, CNRS, Université Paris-Sud, Université Paris-Saclay, Orsay, France

Contents

1 Structures

The interactive 3d structures can be enabled by clicking on them. Flash player is required. Online PDF viewers are often not capable of displaying the structures. If problems arise with other PDF viewers Adobe Acrobat always worked in our testing.

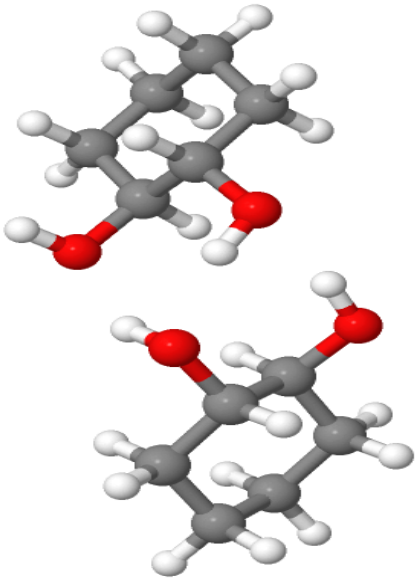

(a) hom3'

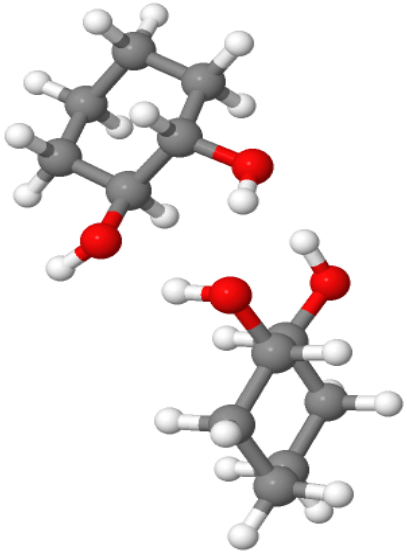

(b) hom3

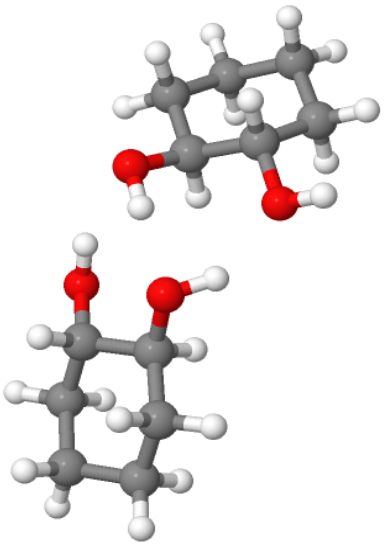

(c) hom3a

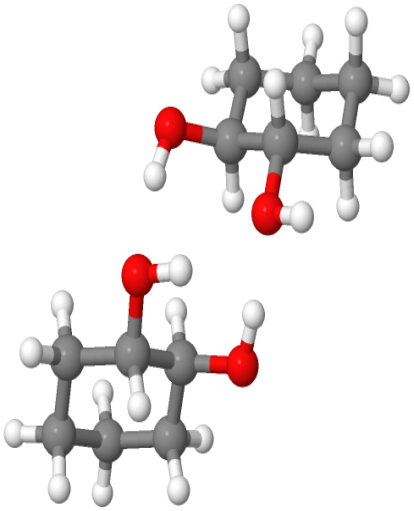

(d) hom3$'_b$

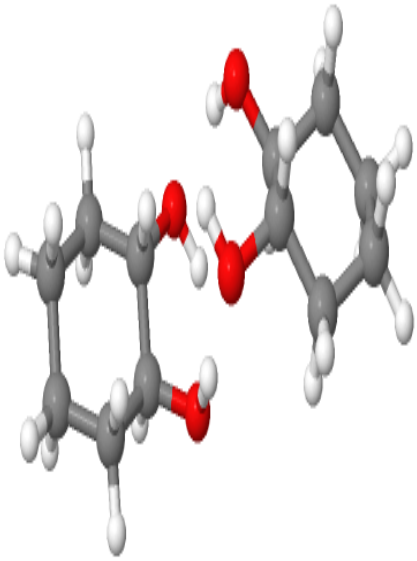

(e) hom2"

Fig. S1.1: Interactive 3d representation of the relevant homo-dimers of CD. The shown CD structures are closely related to the corresponding ED structures.

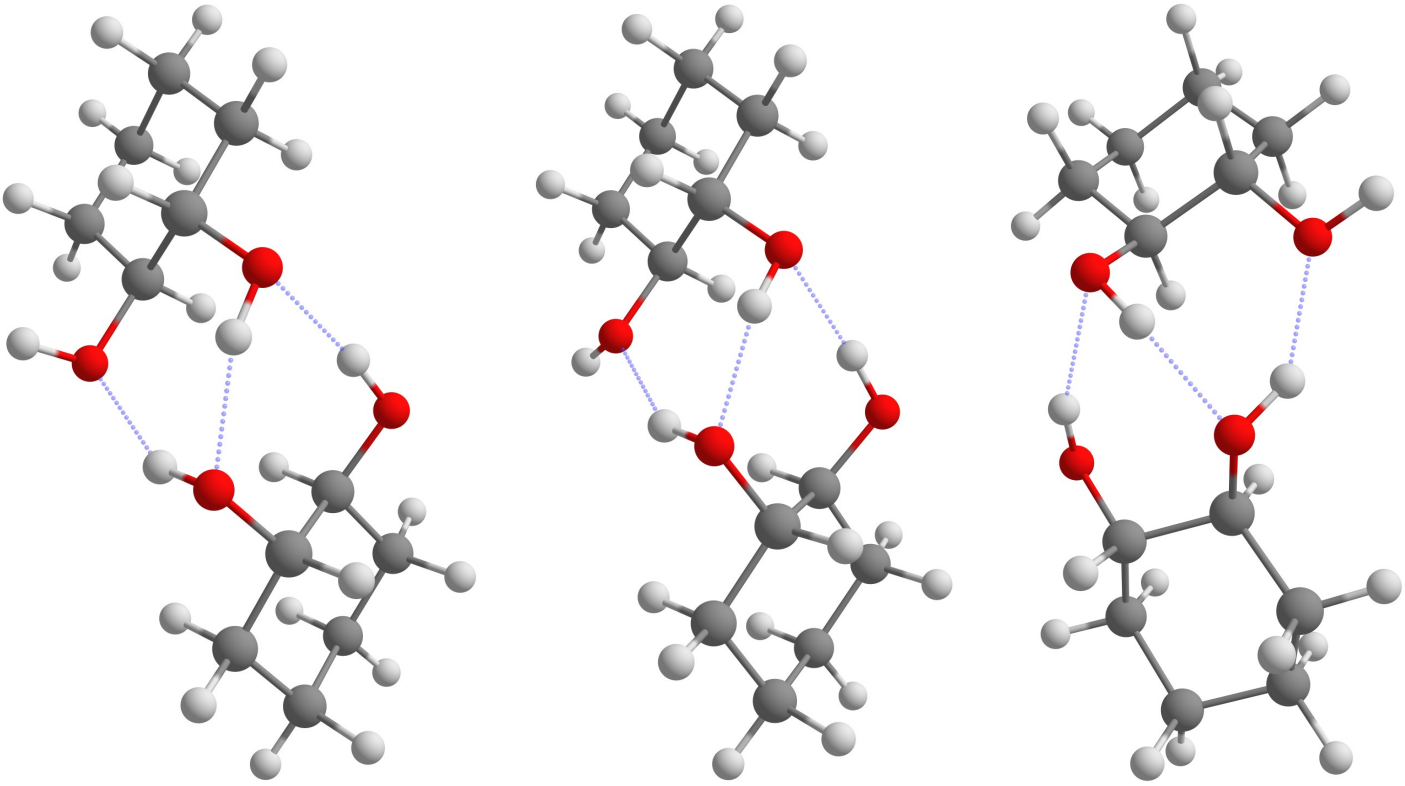

(a) hom3’ (b) hom3 (c) hom3a

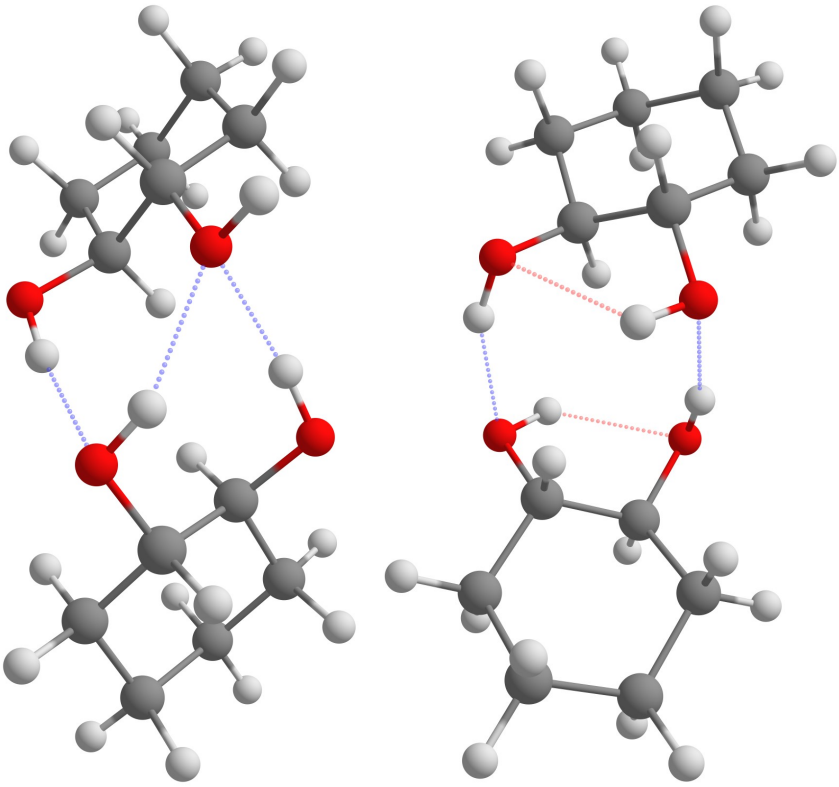

(d) hom3$'_b$ (e) hom2”

Fig. S1.1a: Static representations of the relevant homo-dimers of CD. The shown CD structures are closely related to the corresponding ED structures. Blue dashed lines indicate intermolecular hydrogen bonds and red ones intramolecular ones.

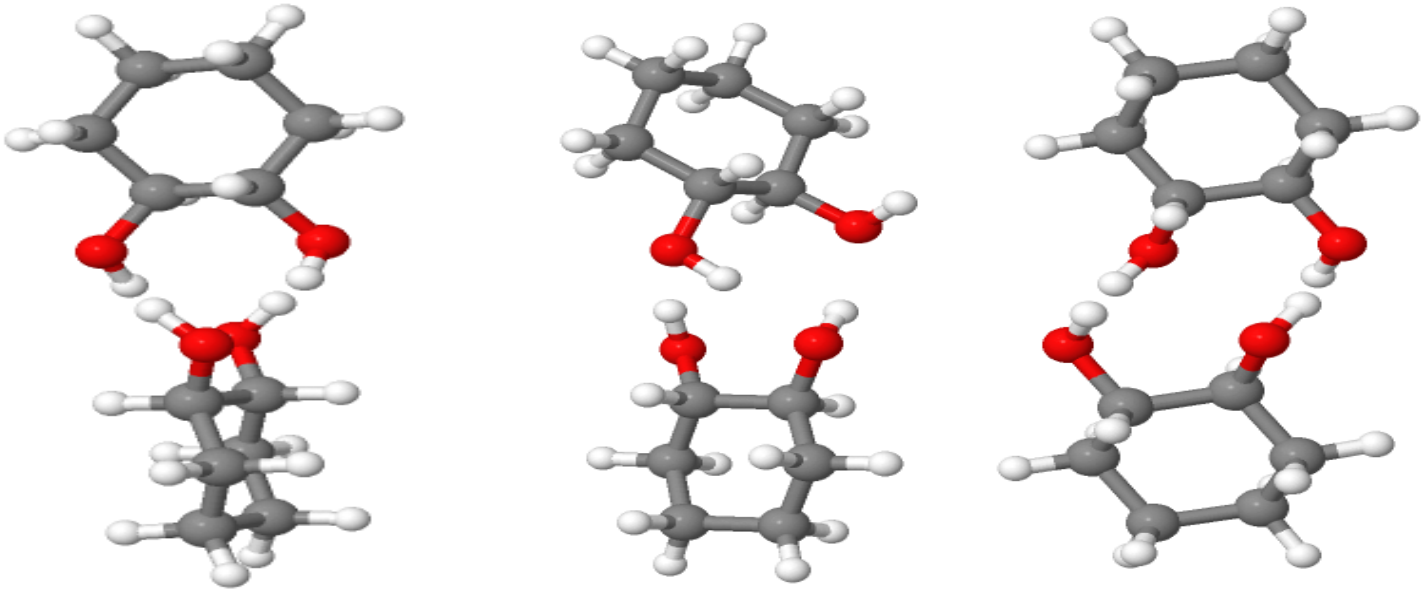

(a) het4 (b) het3' (c) het2"

Fig. S1.2: Interactive 3d representation of the three most stable hetero-dimers of CD. The shown CD structures are closely related to the corresponding ED structures.

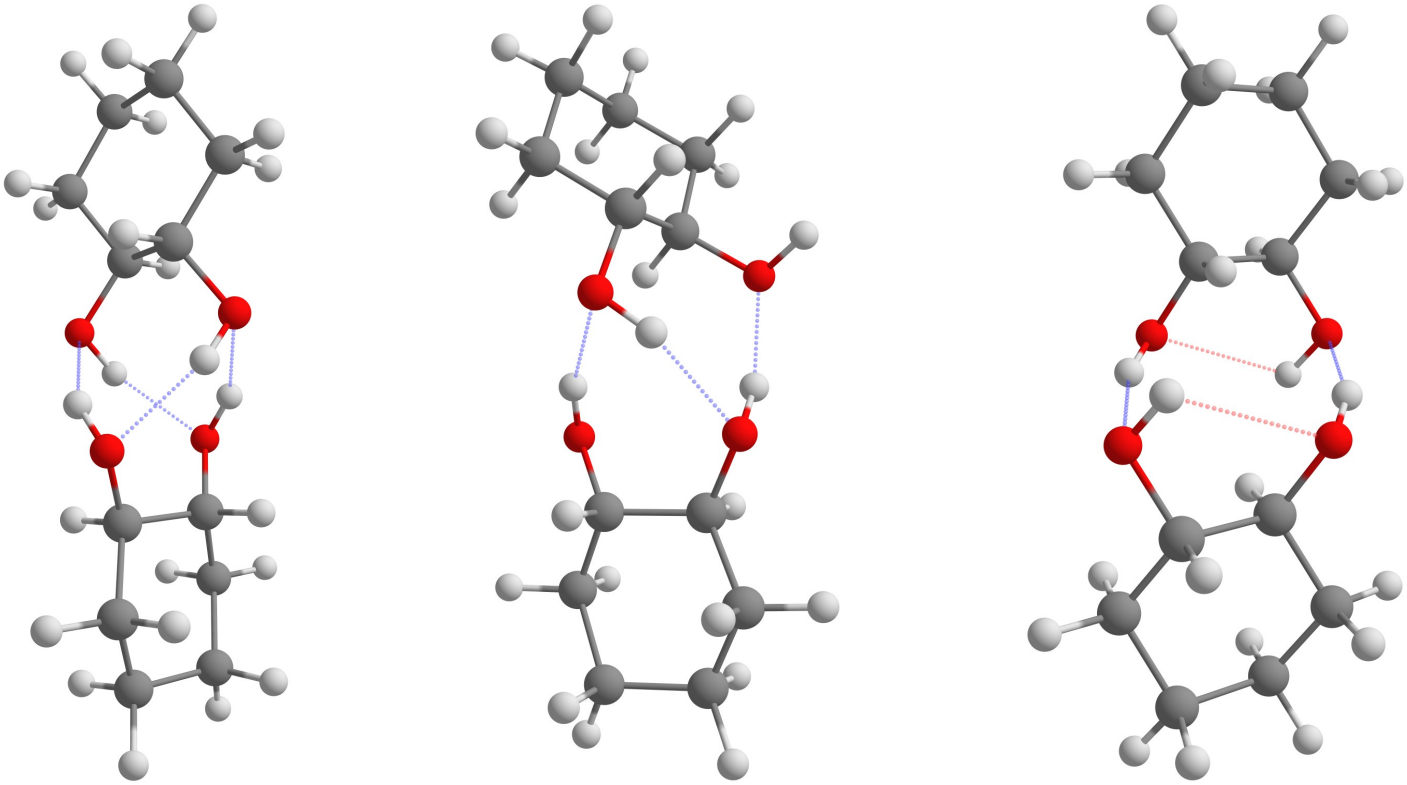

(a) het4 (b) het3' (c) het2

Fig. S1.2a: Static representations of the relevant hetero-dimers of CD. The shown CD structures are closely related to the corresponding ED structures. Blue dashed lines indicate intermolecular hydrogen bonds and red ones intramolecular ones.

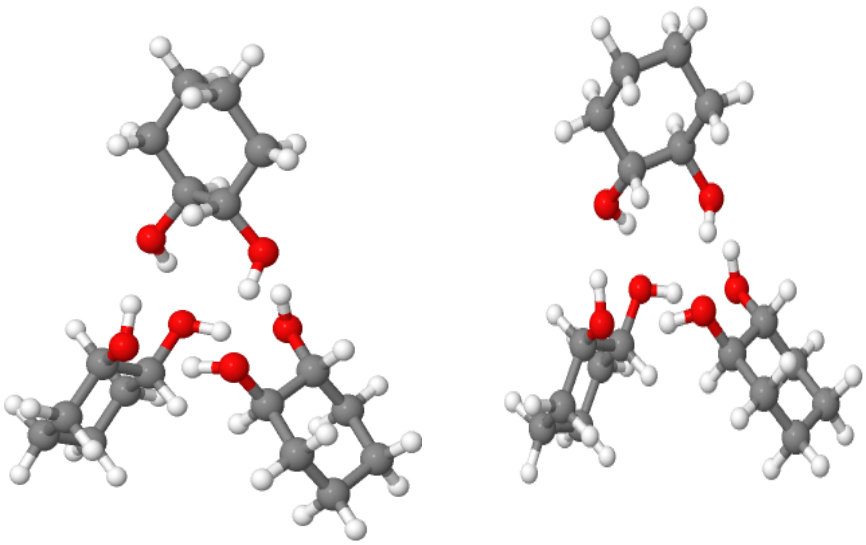

(a) het6 (b) hom6

Fig. S1.3: Interactive 3d representation of the most stable homo- and hetero trimer of CD. The shown CD structures are closely related to the corresponding ED structures.

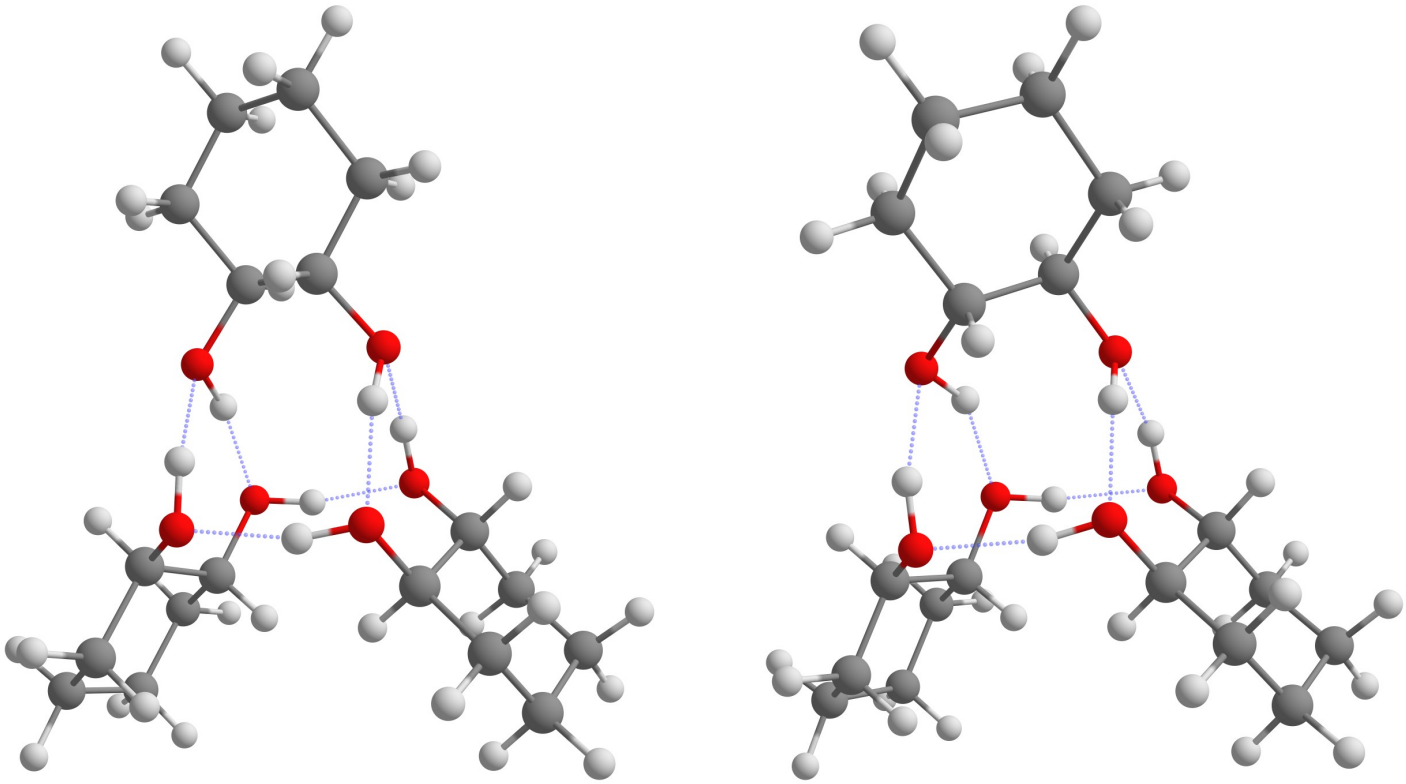

(a) het6 (b) hom6

Fig. S1.3a: Static representations of the most stable homo- and hetero-trimer of CD. The shown CD structures are closely related to the corresponding ED structures. Blue dashed lines indicate intermolecular hydrogen bonds.

2 Tables

Tab. S2.1: Comparison of spectroscopic parameters for the ED slit nozzle expansion spectra shown in Fig. S4.1. All experiments involve a KBr broadband beamsplitter, CaF_2 lenses, a 2mm InSb detector and a watercooled globar radiation source. The risotto experiment has a significantly lower stagnation pressure and a significantly higher nozzle temperature at lower spectral resolution, but it yields comparable spectra, suggesting that these parameters are not critical for ED expansions. He consumption is lowest for the risotto-jet parameters despite the longest nozzle.

parameter	popcorn-jet (old) double slit	risotto-jet V-shaped	popcorn-jet (new) V-shaped
experimental parameters			
number of scans	125	135	86
substance temperature / °C	85	200	70
exposure to temperature / h	>2	<0.0002	>2
nozzle temperature / °C	105	205	90
helium pressure / bar	1.5	0.8	1.5
repetition rate / min^{-1}	1	0.7	1
pumping speed / $m^3\,h^{-1}$	500	1200	500
slit nozzle length / mm	10	90	60
slit nozzle width / mm	2×0.5	0.2	0.2
He valve opening time / ms	316	200	200
instrument parameters			
Bruker FTIR spectrometer	IFS 66v/S	Equinox 55	IFS 66v/S
individual scan length / ms	178	62	178
spectrometer pressure / bar	<0.01	1	<0.01
acquisition parameters			
resolution / cm^{-1}	2.0	3.5	2.0
mirror velocity / kHz	80	80	80
frequency range / cm^{-1}	0–15799.83	0–5266.7	0–15799.83
acquisition mode (fast return)	double sided	single sided	double sided
optic parameters			
filter range / cm^{-1}	2860–4000	2500–4100	2860–4000
aperture / mm	4	5	4
average nozzle-beam distance / mm	5–6	4–5	4–5

Tab. S2.2: Example inputs for the ORCA calculations. The *X* in def2-*X*ZVP can stand for T or Q depending on the desired basis set.

type of calculation	input
pre-optimisation	`!B97-3c abc TightOpt TightSCF Grid3 FinalGrid5`
optimisation + frequency calculation	`!B3LYP D3BJ abc RIJCOSX def2/J def2-XZVP TightOpt TightSCF NumFreq Grid3 FinalGrid5 GridX4` `% elprop Polar 1 end`

transition state optimisation	`!B3LYP D3BJ abc RIJCOSX def2/J def2-XZVP SlowConv OptTS TightSCF Grid3 FinalGrid5 GridX4 NumFreq`
	`%geom`
	`Calc_Hess true`
	`Recalc_Hess 3 end`

Tab. S2.3: Conformational temperatures T_{conf} in K of ED and CD for M' estimated from the free (F) OH-stretching vibration of M and the intramolecularly bound (B) M' OH-stretching mode in the experimental Raman and FTIR spectra. For CD, the comparison of bound modes suffers from spectral overlap. T_{conf} represents the Boltzmann temperature at which the M' population relative to M corresponds to the observed intensity ratio, neglecting differences in rotational and vibrational partition function. It requires calculated double-harmonic Raman cross-sections ratios and energy differences between the conformations. The underlying electronic (ΔE_{el}) and zero point corrected (ΔE_0) energies are given in kJ mol^{-1} relative to M, which remains the most stable conformer in all cases. The temperatures at the B3LYP-D3/def2-TZVP ($T_{\mathrm{conf}}^{\mathrm{TZVP}}$) and B3LYP-D3/def2-QZVP ($T_{\mathrm{conf}}^{\mathrm{QZVP}}$) levels are given for zero point corrected (no parentheses) and uncorrected (in parentheses) energies. It can be seen that the effect of the zero point energy is quite significant, especially in the case of CD where it leads to unreasonably low T_{conf} for the electronic energy difference. After zero point correction, all conformational temperatures fall in a reasonable range (90–160 K), indicating that the calculated intensity ratios, electronic energy differences and zero point energy corrections are not too far from reality or profit from systematic error compensation. All temperatures >30 K are rounded to the nearest multiple of ten.

		ED		CD	
		TZVP	QZVP	TZVP	QZVP
ΔE_0 (ΔE_{el})		1.053 (0.640)	1.302 (0.947)	0.696 (0.004)	0.952 (0.329)
Spectrum	Bands	ED $T_{\mathrm{conf}}^{\mathrm{TZVP}}$	ED $T_{\mathrm{conf}}^{\mathrm{QZVP}}$	CD $T_{\mathrm{conf}}^{\mathrm{TZVP}}$	CD $T_{\mathrm{conf}}^{\mathrm{QZVP}}$
Raman	M_F/M'_B	110 (80)	130 (100)	100 (0.5)	130 (40)
	M_B/M'_B	90 (50)	110 (80)	-	-
IR	M_F/M'_B	130 (80)	160 (110)	100 (0.6)	150 (50)
	M_B/M'_B	130 (80)	150 (110)	-	-

Tab. S2.4: Overview of calculated energies ΔE of M' relative to M from this work ([a]) and from the literature for ED and CD. All energies are given in kJ mol^{-1}. The LCCSD(T0)-F12a calculations were conducted with the Molpro 2012.1 ab initio programm package[1].

Method		ED	CD
B3LYP-D3(BJ,abc)/def2-TZVP[a]	ΔE_{el}	0.6	0.0
	ΔE_0	1.1	0.7
B3LYP-D3(BJ,abc)/def2-QZVP[a]	ΔE_{el}	1.0	0.3
	ΔE_0	1.3	1.0
B3LYP/6-31+G(d,p)[2]	ΔE_0	1.5	-
B3LYP/6-311++G**[3]	ΔE_0	2.4	-
B3LYP-D3(BJ)/6-311+G(2d,p)[4]	ΔE_0	1.4	-
B3LYP/aug-cc-pVDZ[3]	ΔE_0	1.7	-
B3LYP/aug-cc-pVTZ[5]	ΔE_0	1.8	-
MP2/6-311G**[6]	ΔE_{el}	0.3	-
MP2/6-311G(d,p)[7]	ΔE_{el}	0.3	-
MP2/6-311++G(d,p)[7]	ΔE_{el}	2.6	-
MP2/cc-pVDZ[8]	ΔE_{el}	−0.2	-
MP2/cc-pVDZ[7]	ΔE_{el}	1.8	-
MP2/aug-cc-pVDZ[7]	ΔE_{el}	1.8	-
MP2/cc-pVTZ[7]	ΔE_{el}	1.3	-
QCISD/6-311++G(2d,2p)[9]	ΔE_{el}	2.2	-
	ΔE_0	2.5	-
HM-IE[b][7]	ΔE_{el}	1.5	-
CCSD(T)/cc-pVDZ//MP2/cc-pVDZ[8]	ΔE_{el}	−0.5	-
CCSD(T)/aug'-cc-pVTZ[c][5]	ΔE_{el}	1.3	-
LCCSD(T0)-F12a/cc-pVDZ-F12[a]	ΔE_{el}	1.9	-
	ΔE_0	2.0	-
B3LYP/6-311++G**[10]	ΔE_{el}	-	1.3
PBE0/6-311+G(d,p)[11]	ΔE_{el}	1.8	0.8
	ΔE_0	2.0	1.2

[b]hybrid method according to [12], [c]aug-cc-pVTZ on hydroxylgroups otherwise cc-pVTZ

Tab. S2.5: Comparison of the electronic ΔE_{el} and ZPE-corrected relative energy ΔE_0 as well as the accumulated OH-stretching Raman v_{Ra} and IR visiblity v_{IR}, normalised with respect to het4, of the 11 lowest dimer structures of ED and CD for different basis sets (def2-XZVP, X=T, Q) at the B3LYP-D3 level of approximation. Each dimer of CD is structurally related to the corresponding ED dimer.

dimer	XZVP	CD				ED			
		ΔE_{el}	ΔE_0	v_{Ra}	v_{IR}	ΔE_{el}	ΔE_0	v_{Ra}	v_{IR}
het4	T	0.0	0.0	1.00	1.00	0.0	0.0	1.00	1.00
	Q	0.0	0.0	1.00	1.00	0.0	0.0	1.00	1.00
het2"	T	11.6	8.1	0.76	0.59	14.9	10.3	0.97	0.74
	Q	11.0	6.2	0.78	0.61	13.7	9.1	0.97	0.81
het3'	T	11.4	7.6	1.07	0.89	10.8	7.5	1.21	0.98
	Q	9.9	6.4	1.07	0.86	9.4	6.5	1.19	1.00
hom3'	T	12.2	8.2	0.94	0.81	12.2	8.3	1.20	0.92
	Q	10.7	7.1	0.95	0.80	10.4	7.0	1.19	0.93
hom2"	T	11.4	8.0	0.65	0.57	14.6	11.3	1.08	0.76
	Q	11.0	7.4	0.68	0.59	13.9	10.7	0.93	0.77
$hom3_b$'	T	13.2	9.0	0.99	0.71	15.3	10.5	1.27	0.79
	Q	11.4	7.6	0.99	0.68	12.7	8.6	1.23	0.80
$het3_b$'	T	13.8	9.6	1.11	0.75	15.9	10.9	1.25	0.74
	Q	12.0	8.1	1.11	0.74	13.7	9.2	1.22	0.79
hom3	T	13.7	9.5	1.00	0.86	12.8	8.8	1.20	0.94
	Q	12.5	8.7	0.98	0.81	11.2	7.7	1.19	0.94
hom2"a	T	14.6	11.5	0.64	0.61	16.5	12.4	0.98	0.81
	Q	12.1	9.5	0.64	0.59	14.1	10.1	1.00	0.85
hom3a	T	15.1	10.9	1.05	0.81	14.2	9.7	1.31	0.88
	Q	13.8	9.6	1.09	0.80	12.3	8.4	1.28	0.92
hom4	T	12.3	9.7	0.95	0.96	12.6	10.1	1.03	0.95
	Q	12.2	9.9	0.97	0.92	12.5	10.0	1.03	0.97

Tab. S2.6: Experimental band positions in descending wavenumber order with the corresponding assigned structures. Bands labelled M_H are hot bands of M which are discussed in more detail in Fig. S4.4. All values are given in cm^{-1}.

Structure		1	2	3	4
M	ED	3689	3636	-	-
	CD	3667	3628	-	-
M_H	ED	3699	3646	-	-
	CD	-	-	-	-
M'	ED	3656	3623	-	-
	CD	3628	3616	-	-
het4	ED	3513	3475	3475	3444
	CD	3493	3448	3448	3416
hom3'	ED	3670	3526	-	3405
	CD	3644	3511	-	3427
hom2"	ED	-	-	-	-
	CD	-	3565	3511	3427
$hom3_b$'	ED	3670	-	3559	3438
	CD	3644	3591	3535	3448
hom3a	ED	3670	3559	-	3405
	CD	-	-	-	-

Tab. S2.7: Comparison of the electronic ΔE_{el} and ZPE-corrected relative energies ΔE_0 of the 15 lowest trimer structures of ED and CD for the def2-TZVP basis set as well as def2-QZVP for ED at the B3LYP-D3 level of approximation. Each trimer of CD is structurally related to the corresponding ED trimer.

trimer	CD		ED			
	TZVP		TZVP		QZVP	
	ΔE_{el}	ΔE_0	ΔE_{el}	ΔE_0	ΔE_{el}	ΔE_0
het6	0.0	0.0	0.0	0.0	0.0	0.0
het5'	9.3	6.7	10.7	7.5	10.6	7.1
$het6_b$	6.7	7.2	11.5	11.1	12.0	11.5
het5	9.5	7.2	11.7	8.9	12.0	8.9
$het6_ba$	9.2	8.1	14.1	12.4	14.8	13.0
$het6_bb$	9.2	8.3	14.1	12.2	14.9	13.1
het6a	9.1	8.4	17.2	15.0	18.6	17.4
hom6	9.2	8.6	11.4	10.1	12.4	10.8
hom5'	10.6	9.1	16.5	14.3	16.5	14.1
$hom6_b$	9.8	9.6	15.6	13.6	16.0	14.1
$hom6_ba$	10.5	10.1	15.8	13.8	15.9	13.8
het6b	11.6	10.5	9.7	8.8	10.3	8.9
$hom6_bb$	12.2	11.2	15.3	13.5	16.1	13.8
het5'a	11.7	11.56	18.0	16.8	18.6	17.4
hom5'a	13.1	11.5	19.4	16.5	19.9	17.8

Tab. S2.8: Overview of experimental ($\tilde{\nu}_{\mathrm{M,M'}}$) and harmonic computational ($\tilde{\omega}_{\mathrm{M,M'}}$) results for the wavenumbers of the monomer bands of CD from this work ([a]) and from the literature. The experimental downshifts $-\Delta\tilde{\nu}$ result from the formation of the intramolecular hydrogen bond or contact for M and M'. In solution it is not possible to distinguish between the free (1) and bound (2) OH stretching modes of M and those of M'. Therefore the table only lists them as bands of M for simplicity. The computational data is unscaled. Jesus et al. originally scaled their computational data with $\times 0.948$[10]. All values are given in cm^{-1}. CCl_4 attenuates the free/bound splitting, $CDCl_3$ enhances it, whereas all absolute wavenumbers are reduced by solvent or matrix embedding. The PCM model[10] does not reproduce the splitting attenuation and significantly underestimates the absolute wavenumber reduction by CCl_4.

experimental method	$\tilde{\nu}_{\mathrm{M,1}}$	$\tilde{\nu}_{\mathrm{M,2}}$	$\tilde{\nu}_{\mathrm{M'},1}$	$\tilde{\nu}_{\mathrm{M'},2}$	$-\Delta\tilde{\nu}_{\mathrm{M}}$	$-\Delta\tilde{\nu}_{\mathrm{M'}}$
Raman/Jet[a]	3667	3628	3628	3616	39	12
FTIR/Matrix Ar[13] (peak average)	3654	3618	-	-	36	-
IR/CCl_4[10]	3631	3598	-	-	33	-
IR/CCl_4[14]	3634	3602	-	-	32	-
IR/CCl_4[15]	3633	3601	-	-	32	-
IR/CCl_4[16]	3632	3598	-	-	34	-
FTIR/CCl_4[13]	3631	3598	-	-	33	-
VCD,IR/CCl_4[17]	3632	3600	-	-	32	-
FTIR/$CDCl_3$[13]	3609	3545	-	-	64	-
IR/CS_2[16]	3615	3588	-	-	27	-
computational method	$\omega_{\mathrm{M,1}}$	$\omega_{\mathrm{M,2}}$	$\omega_{\mathrm{M'},1}$	$\omega_{\mathrm{M'},2}$	$-\Delta\omega_{\mathrm{M}}$	$-\Delta\omega_{\mathrm{M'}}$
B3LYP-D3(BJ,abc)/def2-TZVP[a]	3808	3769	3771	3752	39	19
B3LYP-D3(BJ,abc)/def2-QZVP[a]	3832	3795	3797	3778	37	19
B3LYP/6-311++G**[10]	3842	3804	3807	3788	38	19
B3LYP/6-311++G**[10] (PCM)	3836	3796	3801	3783	40	18

3 Energy Diagrams

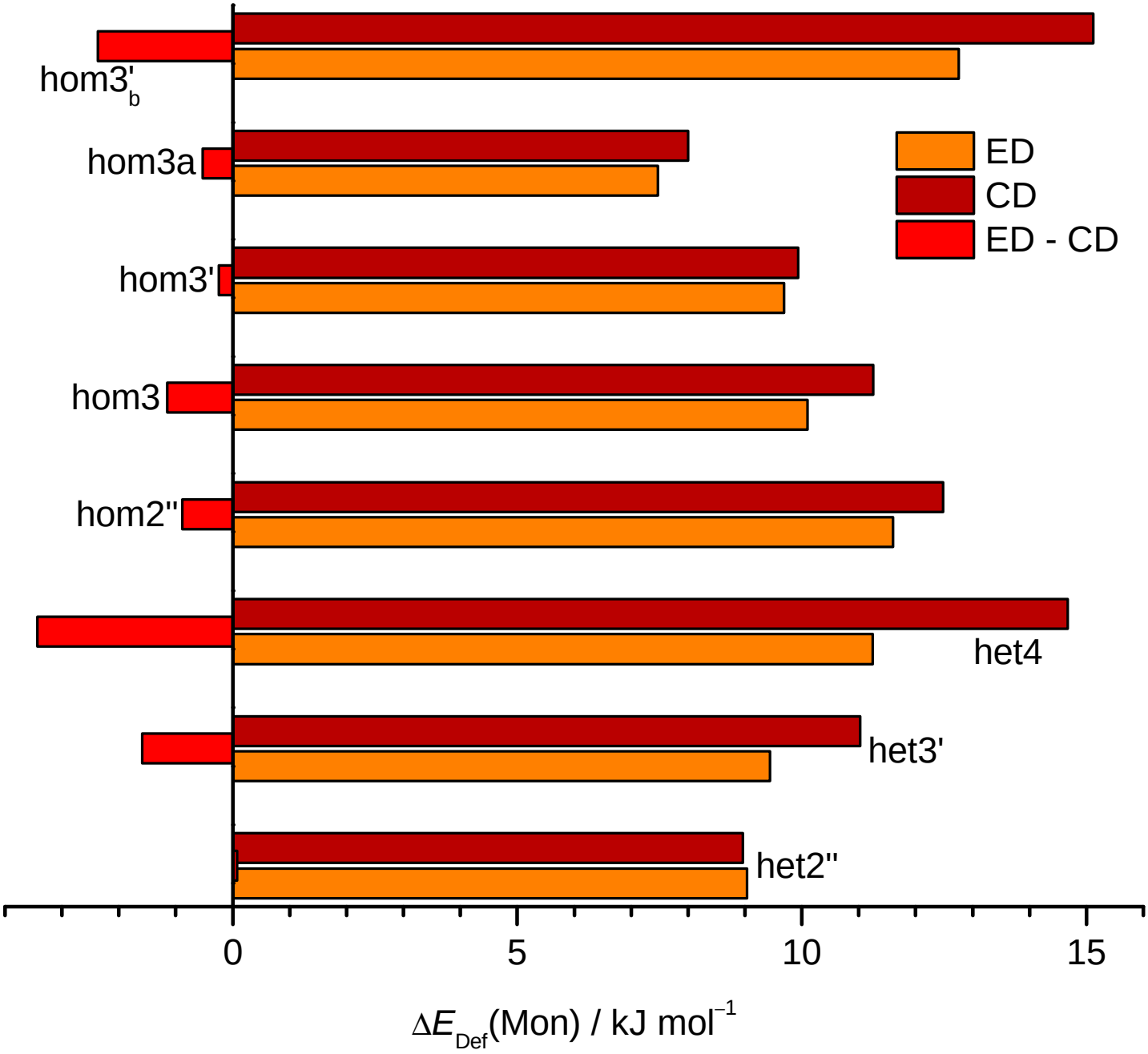

Fig. S3.1: Absolute values for the total deformation energy relative to the most stable monomer (M). The deformation energies for ED are shown in orange, for CD in dark red and the difference of ED and CD in red. It is evident that the increase of the deformation energy when switching from ED to CD is the highest for the strained het4. This effect is also quite pronounced for hom3$_b$' which results from the strongly distorted bifurcated donor monomer subunit. The difference between ED and CD relative to het4 results in the values that were used for Fig. 5 of the paper for the other conformations.

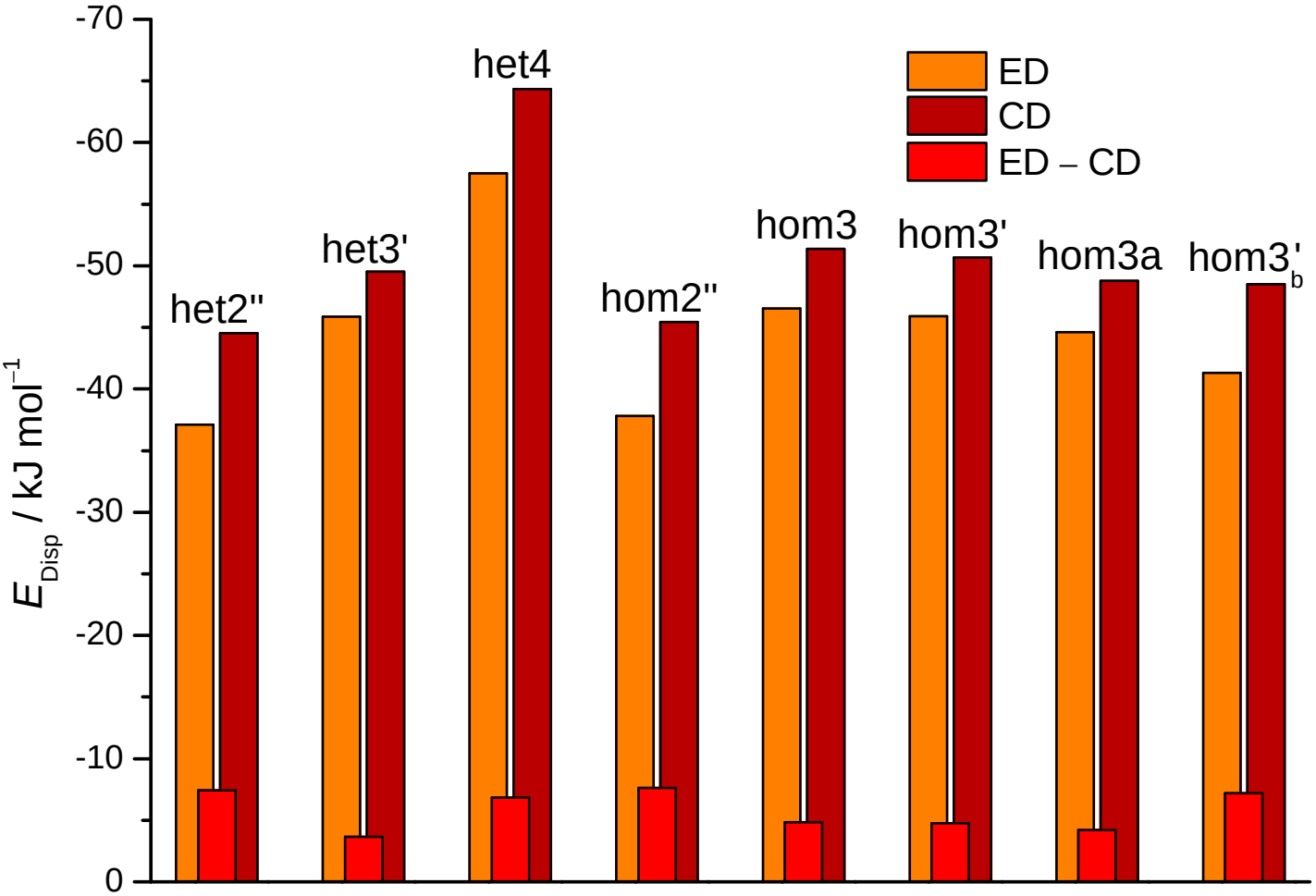

Fig. S3.2: Absolute values for the intermolecular dispersion based on the SAPT2+/aug-cc-pVDZ calculations. The dispersion energies for ED are shown in orange, for CD in dark red and the difference between ED and CD in red. The difference between ED and CD relative to the het4 case results in the dispersion contributions of Fig. 5 in the paper for the other dimer conformations.

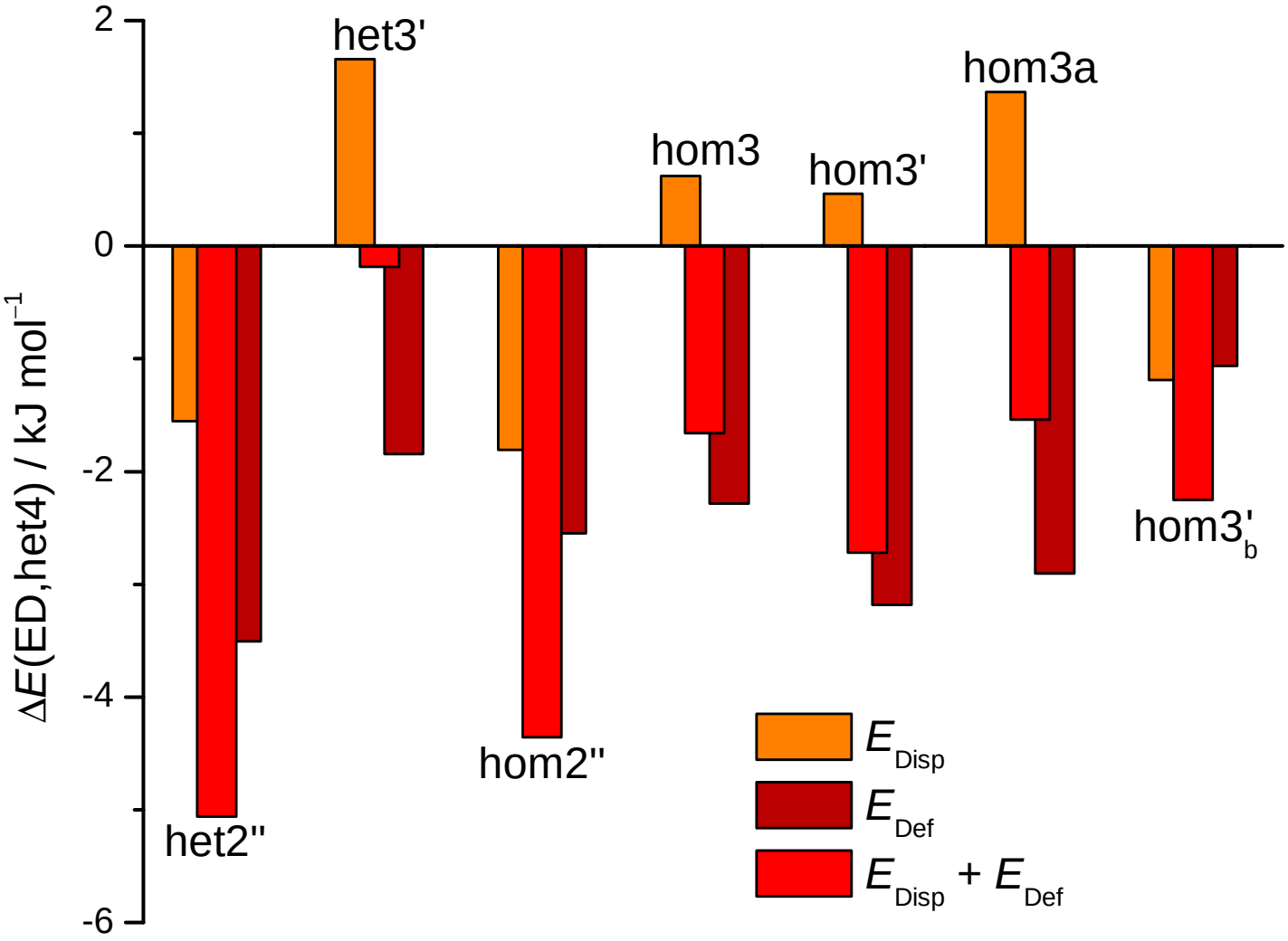

Fig. S3.3: Analogous analysis as in Fig. 6 of the paper but with dispersion energies taken from D3(BJ,abc) calculations. The intermolecular dispersion energies are crudely estimated by performing single point calculations on the monomer subunits and taking the D3(BJ,abc) terms and comparing them to those of the dimer. Qualitatively there are no significant changes in comparison to the SAPT2+ analysis.

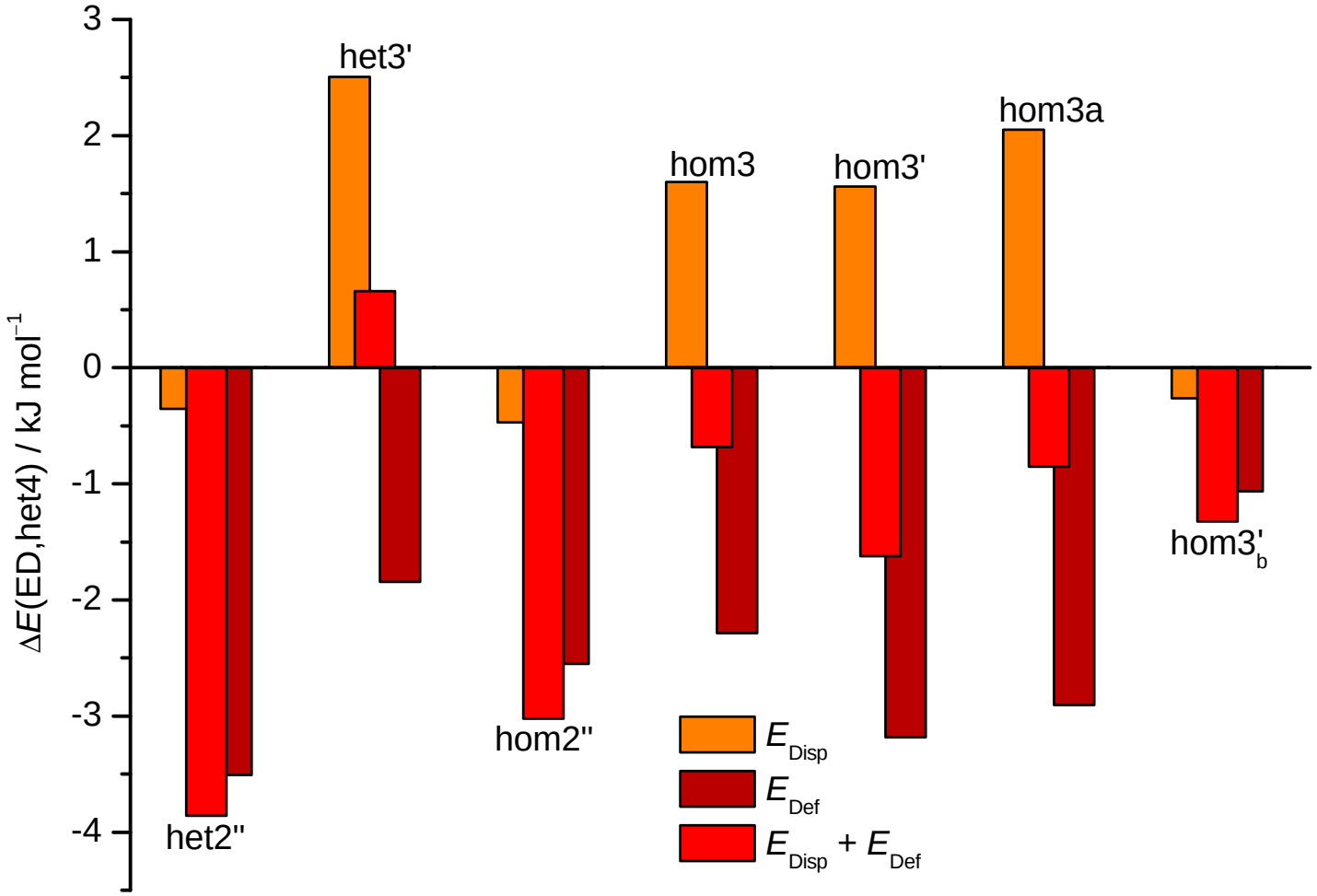

Fig. S3.4: Analogous analysis as in Fig. 6 of the paper but with dispersion energies taken from sSAPT0/jun-cc-pVDZ calculations. Qualitatively there are no significant changes in comparison to the SAPT2+ analysis. The lower case s indicates that some special scaling was applied according to the standard value of Psi4 1.2.1[18], with which the calculations were carried out. Furthermore density fitting was used with all other parameters remaining unchanged with respect to their default settings. It should be noted that the success of sSAPT0/jun-cc-pVDZ is entirely dependent on error compensation and the chosen basis set was based on the recommendation of Parker et al.[19] which yielded the best error compensation in their tests.

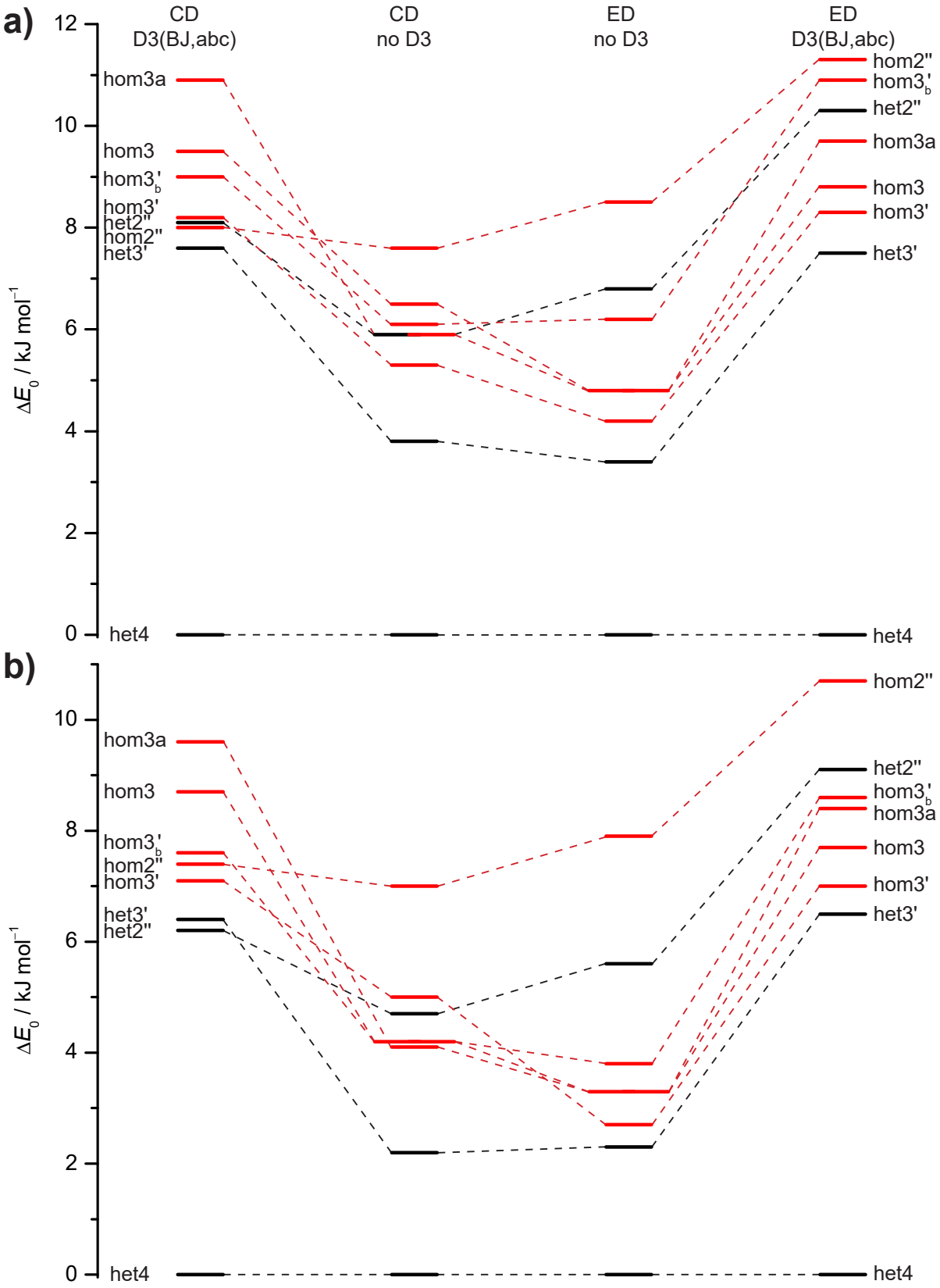

Fig. S3.5: ZPV-corrected relative energies of the ED-dimers (left) and CD-dimers (right) at the B3LYP/def2-TZVP (**a)** and B3LYP/def2-QZVP (**b)** level with (outer) and without D3(BJ,abc) dispersion correction (inner column), distinguished between heterochiral (black) and homochiral (red) pairings. The energy change of the dimers is highlighted by a dashed line in the corresponding colour. Only dimers relevant to the interpretation of the spectra are shown. The stabilisation of all conformers when no dispersion correction is used can be explained by the fact that het4 profits the most from dispersion interactions. The hydrogen bonds are slightly longer which also predominately affects het4 due to the fact that four hydrogen bonds are getting weaker. In case of ED all shifts are fairly equal which is in line with similar dispersion interactions among the conformers. This is also mostly the case for CD with the exception of hom2" and het2", indicating that they themselves also are strongly affected by London forces resulting in a less pronounced stabilisation.

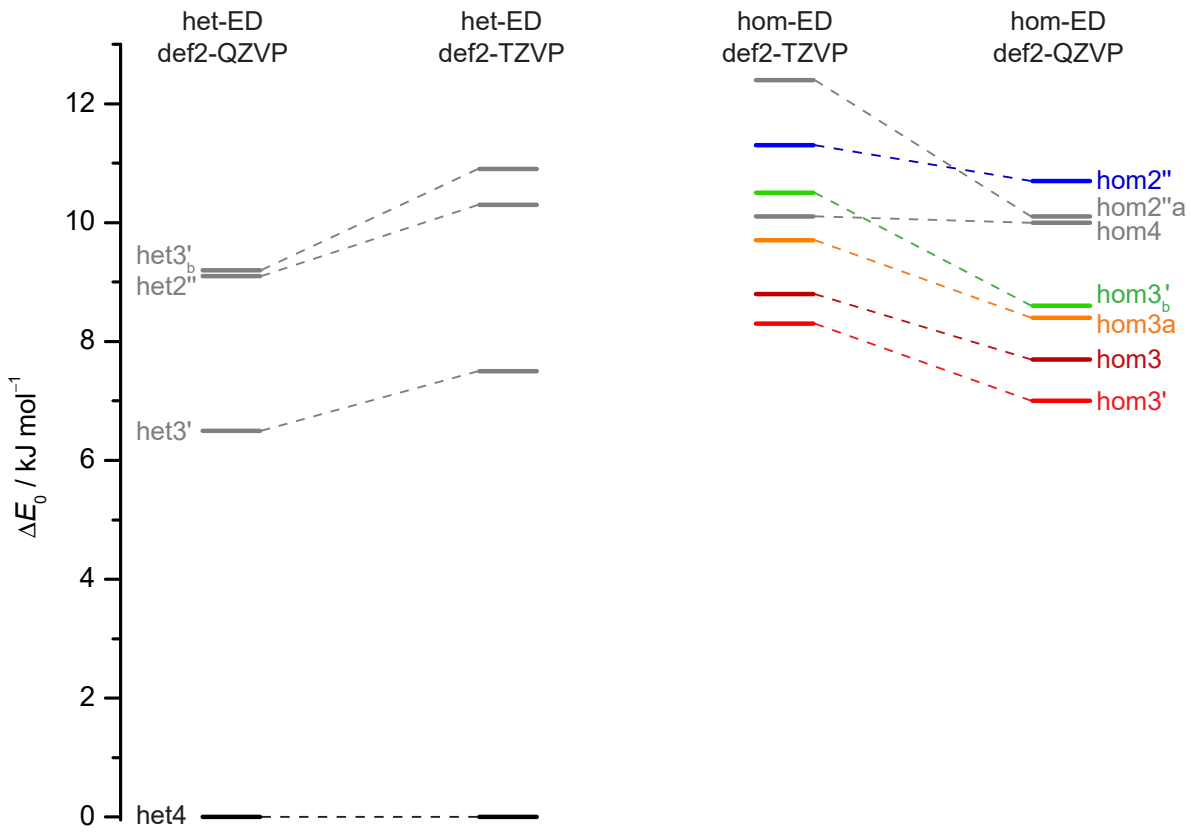

Fig. S3.6: ZPV-corrected relative energies of ED-dimers at the B3LYP/def2-TZVP (inner) and B3LYP-D3/def2-QZVP (outer column) level, distinguished between heterochiral (left) and homochiral (right) pairings.

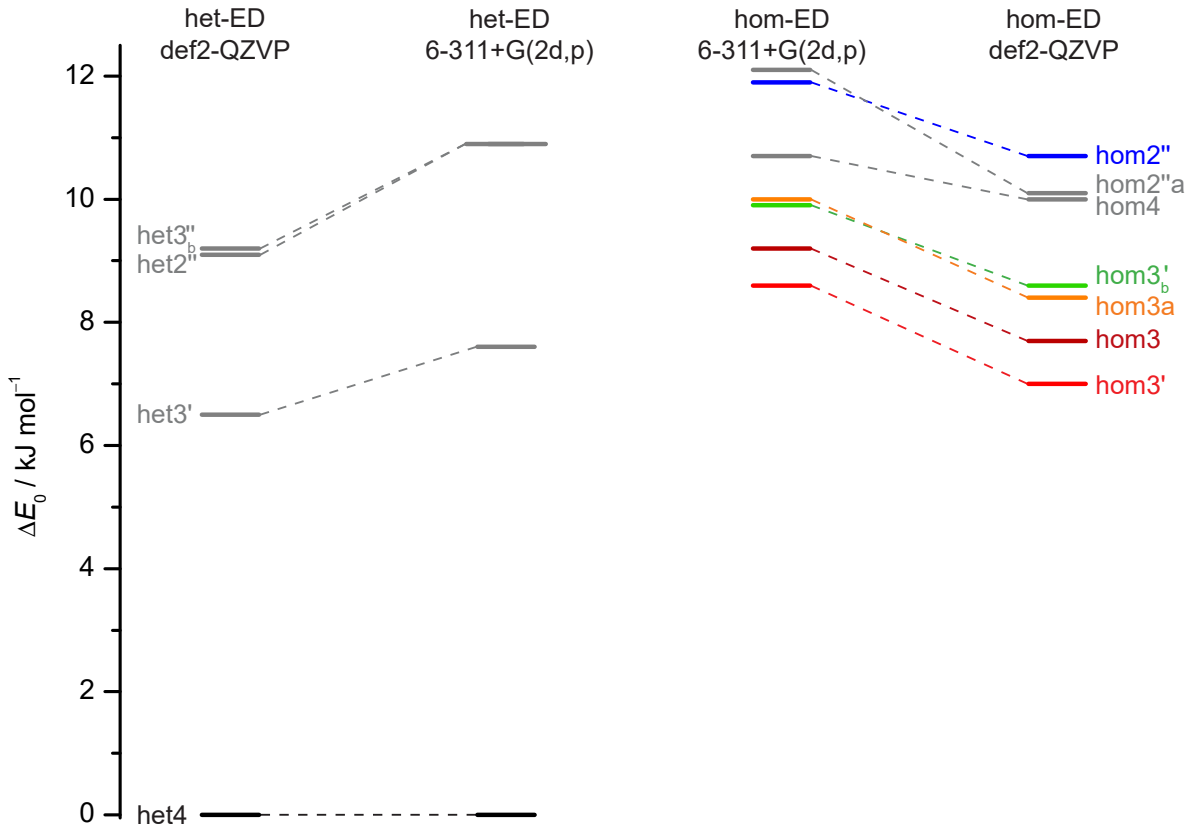

Fig. S3.7: ZPV-corrected relative energies of ED-dimers at the B3LYP/6-311+G(2d,p) (inner) and B3LYP-D3/def2-QZVP (outer column) level of calculation, distinguished between heterochiral (left) and homochiral (right) pairings.

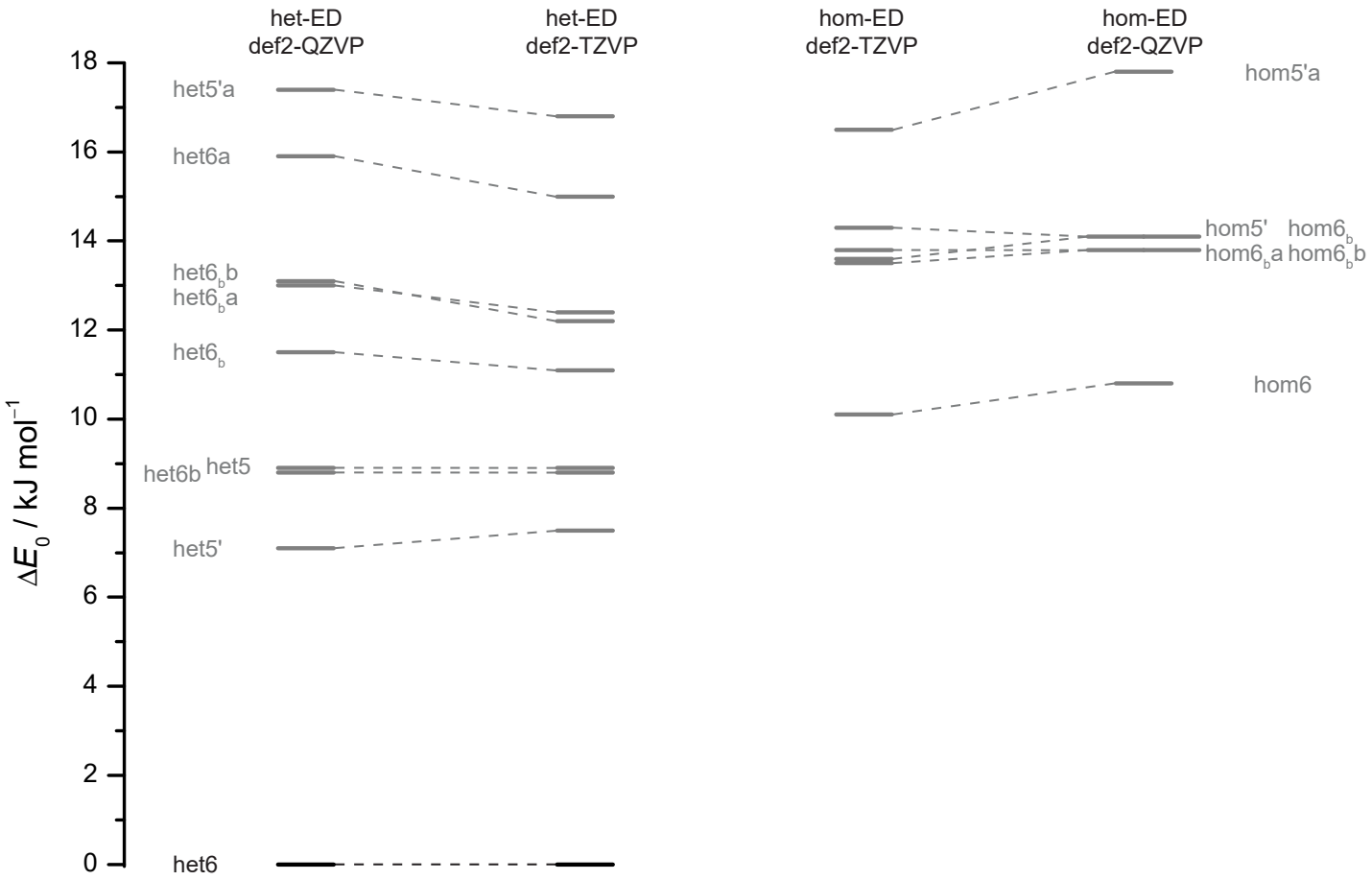

Fig. S3.8: ZPV-corrected relative energies of the ED-trimers at the B3LYP/def2-TZVP (inner) and B3LYP-D3/def2-QZVP (outer column) level of calculation, distinguished between heterochiral (left) and homochiral (right) pairings. The moderate shifts when switching between basis sets indicate that the BSSE, due to the uniformly compact hydrogen bond networks, appears to be less impactful for the trimers than for the dimers.

4 Additional Spectra

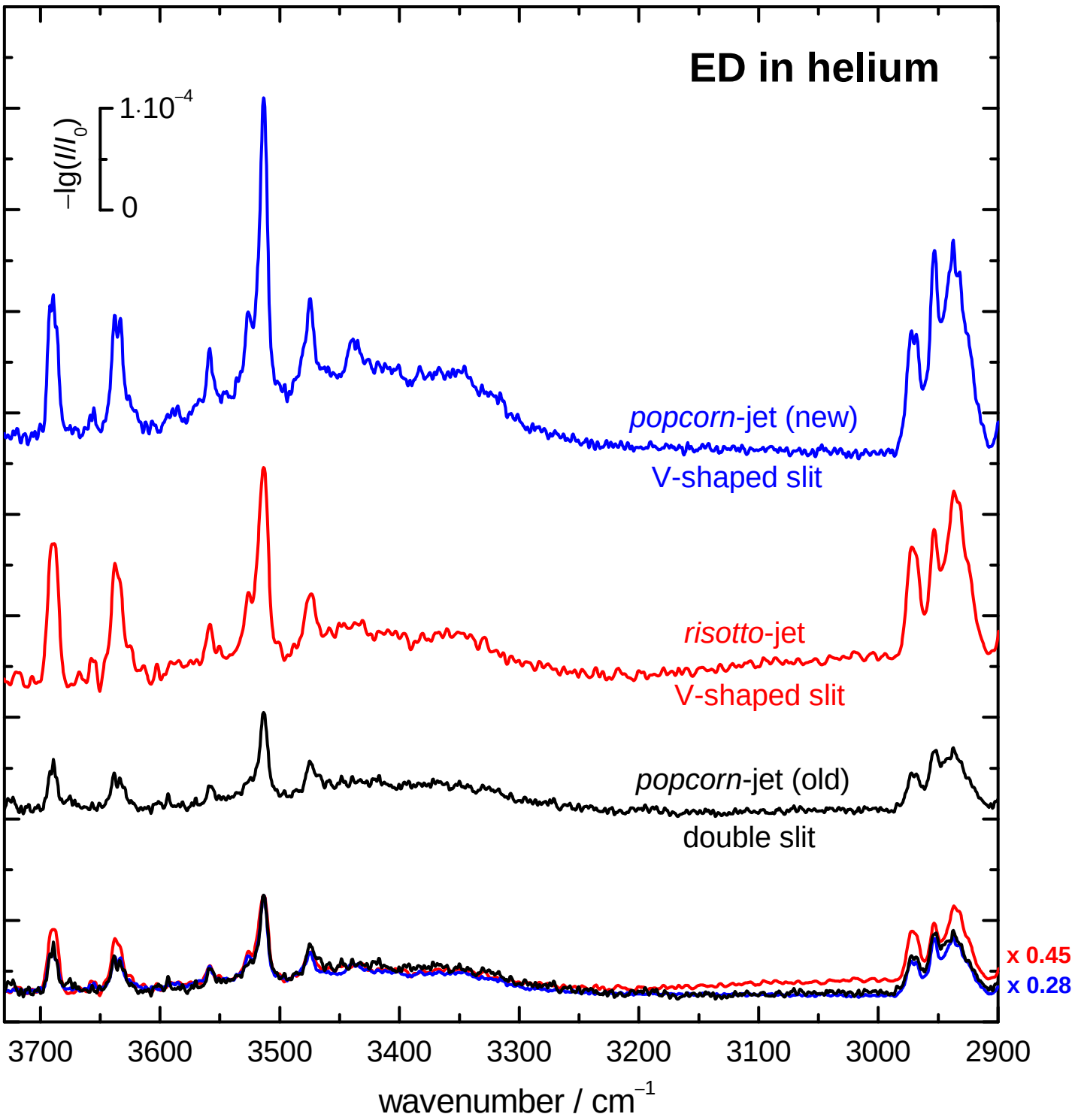

Fig. S4.1: ED expansions in helium with similar cluster composition using the 3 different setups described in the text and characterised in Tab. S2.1. The three dimer-scaled and overlaid bottom traces show that the column density of the new popcorn (risotto) jet expansions has increased about 3-fold (2-fold). The differences in noise in the corresponding unscaled upper traces can be largely attributed to differences in scan number and resolution as well as spectrometer and acquisition mode. Note that the temperatures chosen for the popcorn-jet spectra differ slightly from those in Fig. 2 to maximise the comparability between the three experiments and the cluster composition.

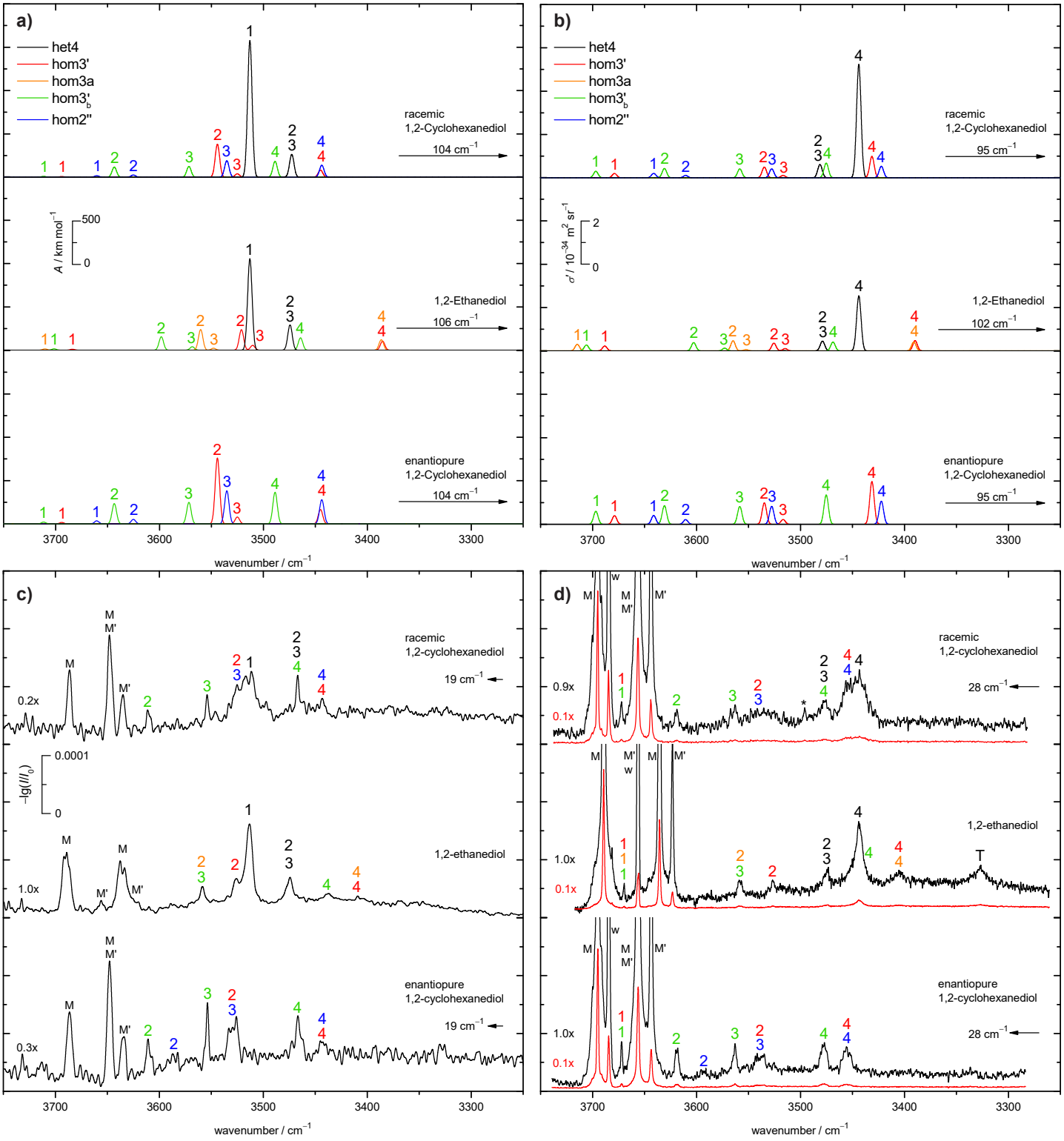

Fig. S4.2: As Fig. 7 in the main text, but for the B3LYP-D3(BJ,abc)/def2-TZVP level of computation.

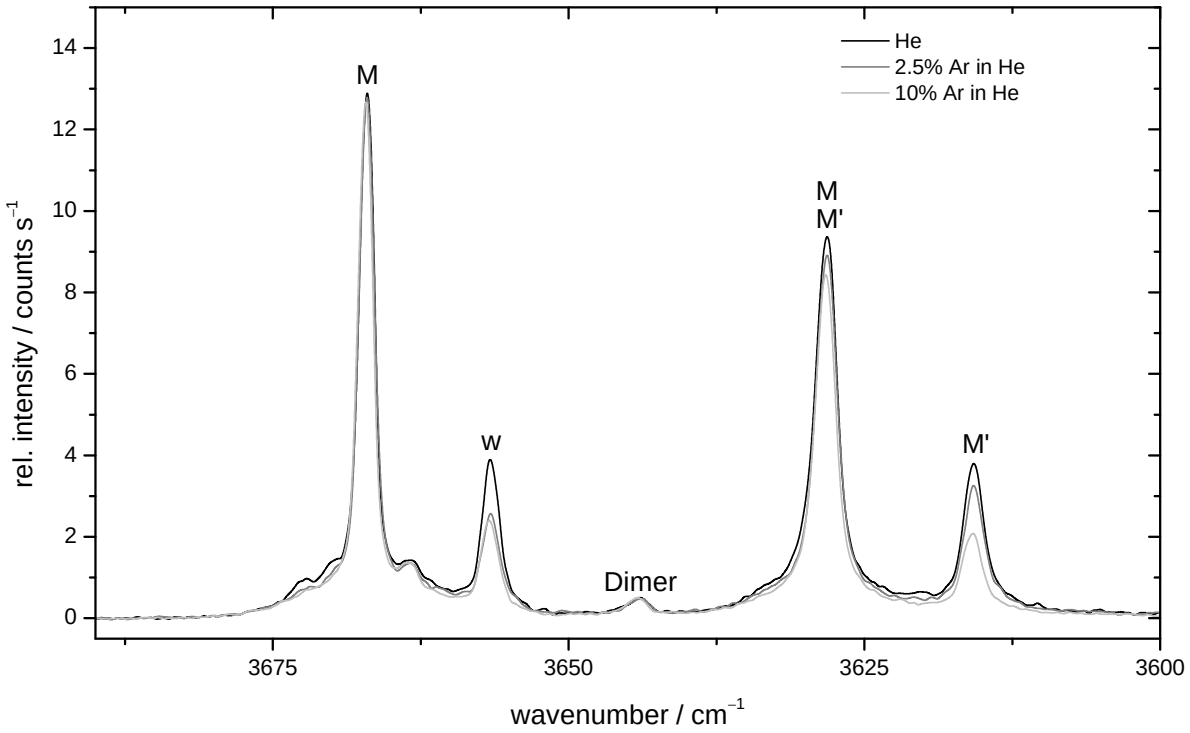

Fig. S4.3: Raman spectra of CD with increasing fractions of argon added to helium as a seeding gas. The spectra are scaled to the non-overlapping M band. As one would expect the overlapping bands of M and M' decrease to a lesser extent than the pure M' band due to the stronger relaxation of the less stable M' monomer when higher concentrations of argon are used. w indicates a band due to water impurities.

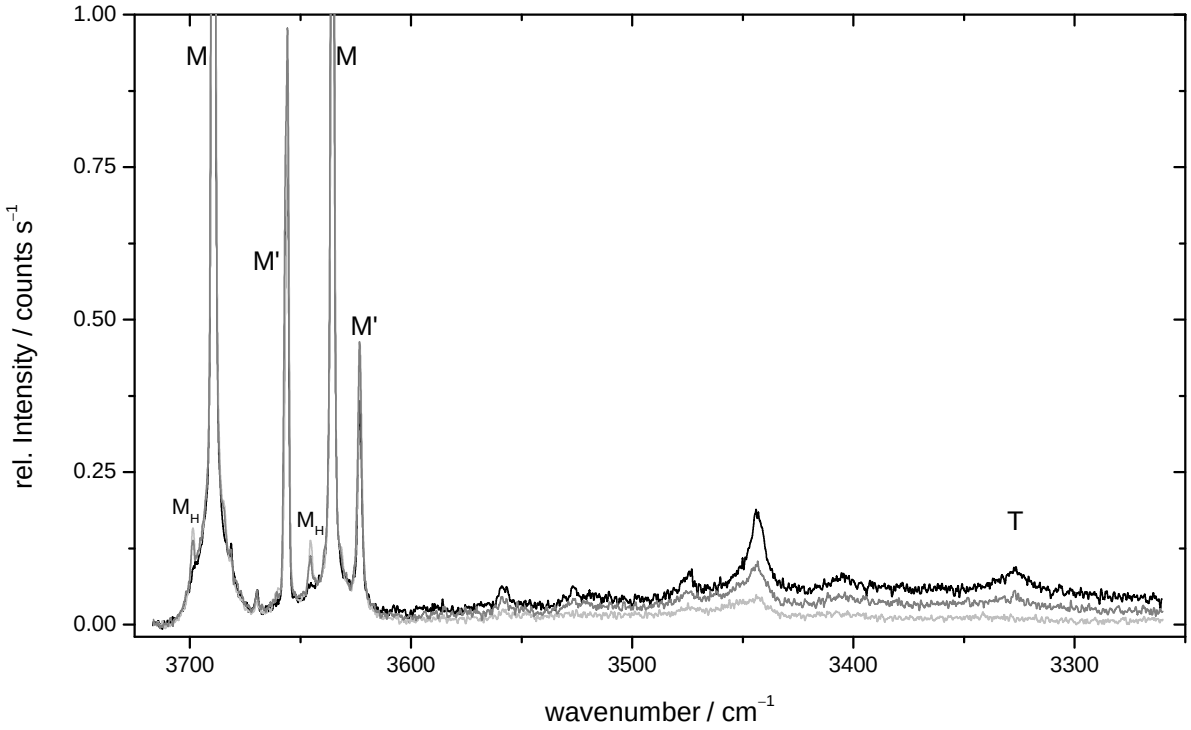

Fig. S4.4: Raman spectra of ED under less favourable clustering conditions going from black to light grey. For the grey spectra the tubing and nozzle temperature was increased and the stagnation pressure decreased. The spectra are scaled to M. The black spectrum is also shown in Fig. 2 of the paper. The spectral features labelled M_H are most likely caused by hot transitions from the corresponding low lying torsional OH-mode ($\tilde{\nu}_{\mathrm{tor}}(v)$) to the OH-stretching mode ($\tilde{\nu}_{\mathrm{OH}}(v)$) of M ($\tilde{\nu}_{\mathrm{OH}}(1) + \tilde{\nu}_{\mathrm{tor}}(1) \leftarrow \tilde{\nu}_{\mathrm{OH}}(0) + \tilde{\nu}_{\mathrm{tor}}(1)$). The observed shifts are in good agreement with a VPT2 calculation at the B3LYP-D3(BJ)/def2-QZVP level of computation performed with Gaussian 09 Rev.E01[20].

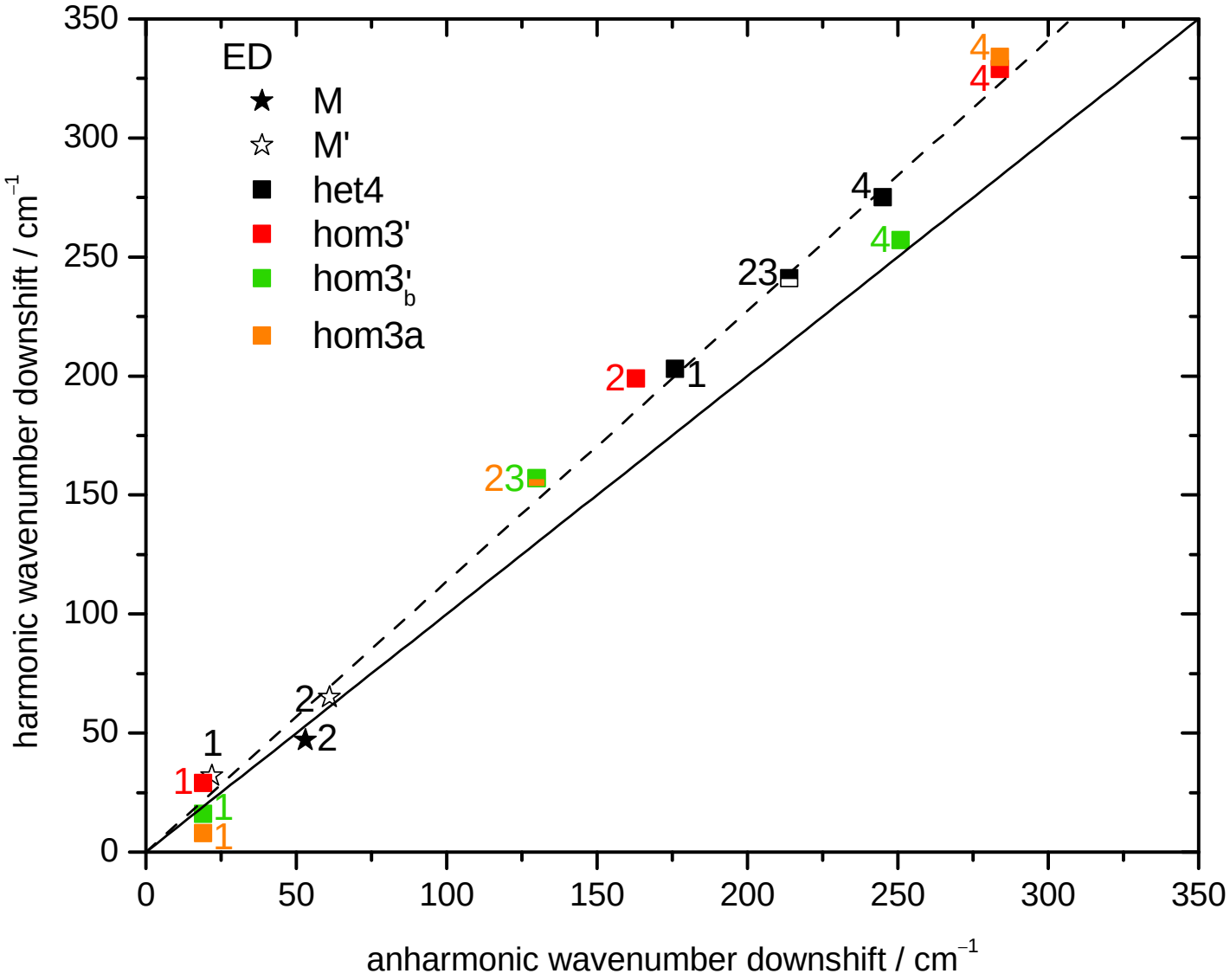

Fig. S4.5: Comparison of the theoretically predicted harmonic frequency downshifts at the B3LYP-D3(BJ,abc)/def2-QZVP level of computation with the anharmonic (i.e. experimental) downshifts of ED. All downshifts are relative to the free OH stretching mode of M. The numbering of the bands is analogous to Fig. 7 of the main text. One can see the systematic relative overestimation of the downshift with increasing magnitude, a slight exception being the anticooperative bonding situation in hom3$'_b$. A linear fit (dashed line) through the origin to all data points has a slope of 1.14.

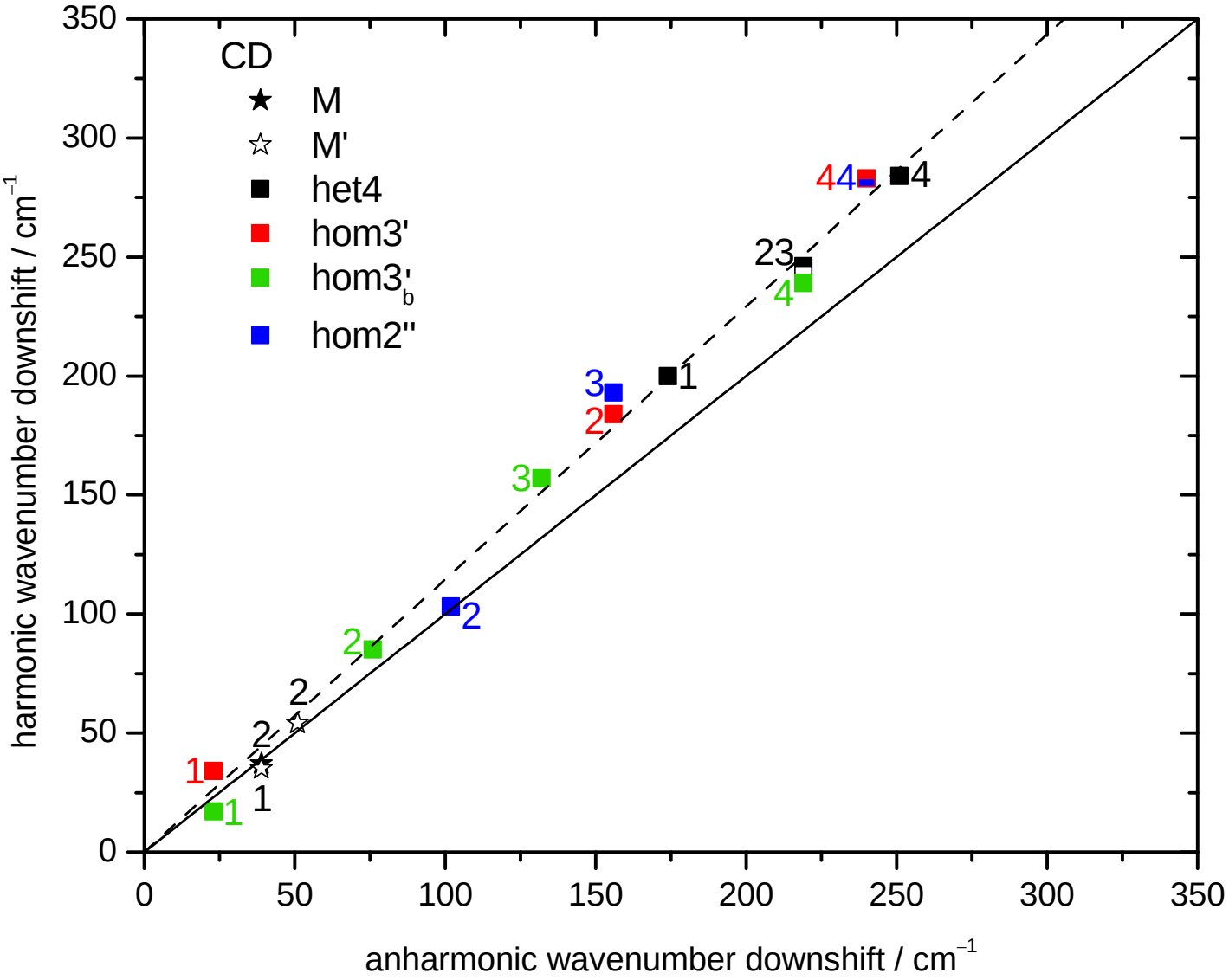

Fig. S4.6: Comparison of the theoretically predicted harmonic frequency downshifts at the B3LYP-D3(BJ,abc)/def2-QZVP level of computation with the anharmonic (i.e. experimental) downshifts of CD. All downshifts are relative to the free OH mode of M. The numbering of the bands is analogous to Fig. 7 of the main text. One can see the systematic relative overestimation of the downshift with increasing magnitude. A linear fit (dashed line) through the origin to all data points has a slope of 1.15.

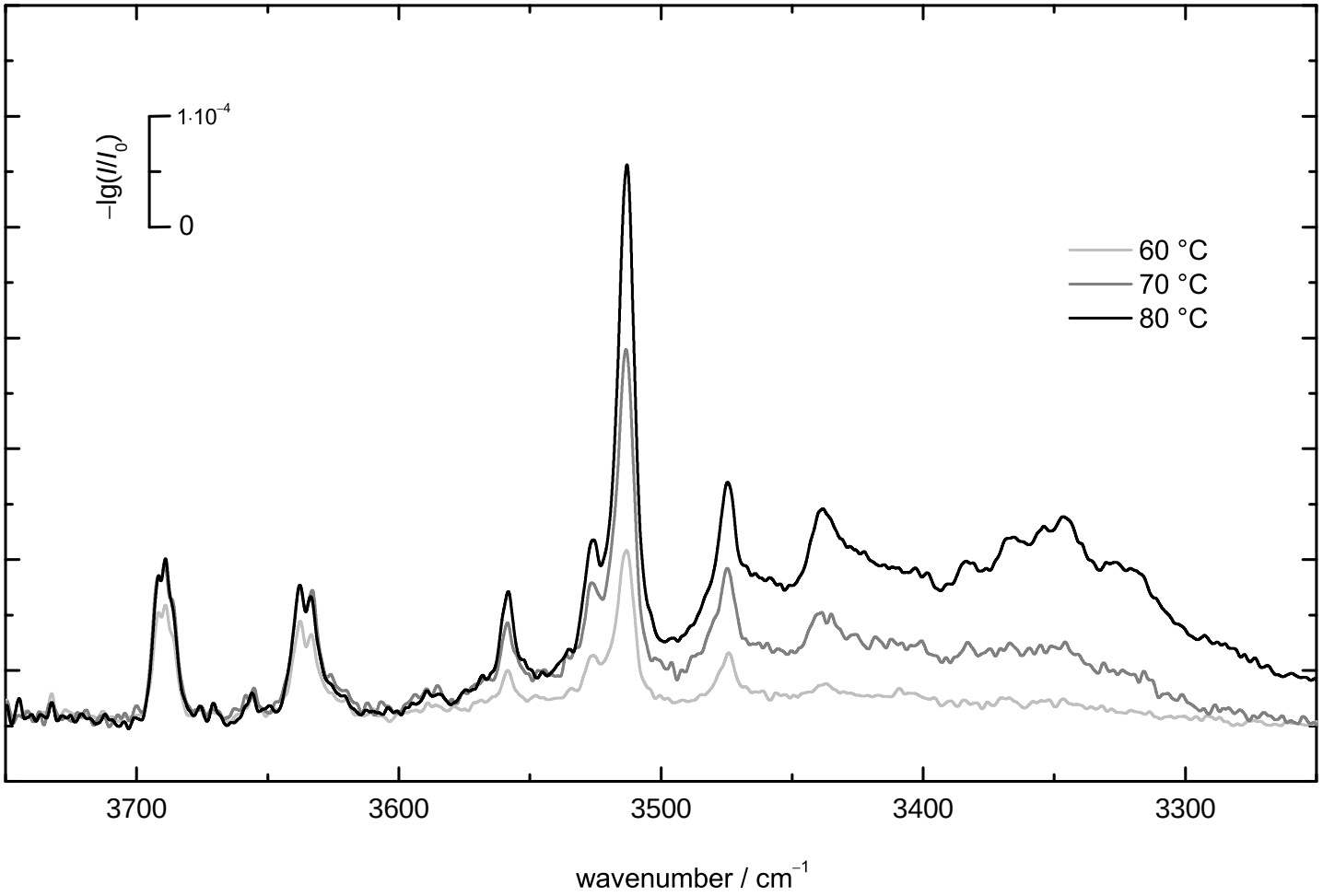

Fig. S4.7: Additional spectra of ED measured with the *popcorn*-jet (new) at sample temperatures of 60 °C (371 scans), 70 °C (86 scans) and 80 °C (176 scans). All spectra are unscaled. The spectrum measured at 60 °C is identical to the one used in Fig. 6 of the paper. When moving towards 70 °C only broad features arise. At even higher temperatures one very broad band dominates the right part of the spectrum which is likely the result of higher oligomers.

References

[1] H.-J. Werner, P. J. Knowles, G. Knizia, F. R. Manby, M. Schütz, "Molpro: A General-Purpose Quantum Chemistry Program Package", *WIREs Comput. Mol. Sci.* **2012**, *2*, 242–253.

[2] K. Takahashi, "Theoretical Study on the Effect of Intramolecular Hydrogen Bonding on OH Stretching Overtone Decay Lifetime of Ethylene Glycol, 1,3-Propanediol, and 1,4-Butanediol", *Phys. Chem. Chem. Phys.* **2010**, *12*, 13950–13961.

[3] P. Das, P. K. Das, E. Arunan, "Conformational Stability and Intramolecular Hydrogen Bonding in 1,2-Ethanediol and 1,4-Butanediol", *J. Phys. Chem. A* **2015**, *119*, 3710–3720.

[4] F. Kollipost, K. E. Otto, M. A. Suhm, "A Symmetric Recognition Motif between Vicinal Diols: The Fourfold Grip in Ethylene Glycol Dimer", *Angew. Chem. Int. Ed.* **2016**, *55*, 4591–4595.

[5] D. L. Howard, P. Jørgensen, H. G. Kjaergaard, "Weak Intramolecular Interactions in Ethylene Glycol Identified by Vapor Phase OH-Stretching Overtone Spectroscopy", *J. Am. Chem. Soc.* **2005**, *127*, 17096–17103.

[6] B. J. Teppen, M. Cao, R. F. Frey, C. van Alsenoy, D. M. Miller, L. Schäfer, "An Investigation into Intramolecular Hydrogen Bonding: Impact of Basis Set and Electron Correlation on the Ab Initio Conformational Analysis of 1,2-Ethanediol and 1,2,3-Propanetriol", *J. Mol. Struct. THEOCHEM* **1994**, *314*, 169–190.

[7] O. Guvench, A. D. MacKerell, "Quantum Mechanical Analysis of 1,2-Ethanediol Conformational Energetics and Hydrogen Bonding", *J. Phys. Chem. A* **2006**, *110*, 9934–9939.

[8] C. J. Cramer, D. G. Truhlar, "Quantum Chemical Conformational Analysis of 1,2-Ethanediol: Correlation and Solvation Effects on the Tendency To Form Internal Hydrogen Bonds in the Gas Phase and in Aqueous Solution", *J. Am. Chem. Soc.* **1994**, *116*, 3892–3900.

[9] D. L. Howard, H. G. Kjaergaard, "Influence of Intramolecular Hydrogen Bond Strength on OH-Stretching Overtones", *J. Phys. Chem. A* **2006**, *121*, 10245–10250.

[10] A. J. L. Jesus, J. S. Redinha, "Self-Association of 1,2-Cyclohexanediols: A Spectroscopic and Computational Study", *J. Mol. Struct.* **2014**, *1067*, 104–111.

[11] J. S. Lomas, "1H NMR Spectra of Ethane-1,2-diol and other Vicinal Diols in Benzene: GIAO/DFT Shift Calculations", *Magn. Reson. Chem.* **2013**, *51*, 32–41.

[12] J. B. Klauda, S. L. Garrison, J. Jiang, G. Arora, S. I. Sandler, "HM-IE: Quantum Chemical Hybrid Methods for Calculating Interaction Energies", *J. Phys. Chem. A* **2004**, *108*, 107–112.

[13] J. F. Bacon, J. H. van der Maas, J. R. Dixon, W. O. George, P. S. McIntyre, "Structural Information from OH Stretching Frequencies—Conformations of Cyclohexanol and Cyclohexandiols", *Spectrochim. Acta A* **1989**, *45*, 1313–1318.

[14] L. P. Kuhn, "The Hydrogen Bond. I. Intra- and Intermolecular Hydrogen Bonds in Alcohols", *J. Am. Chem. Soc.* **1952**, *74*, 2492–2499.

[15] C. W. Davey, E. L. McGinnis, J. M. McKeown, G. D. Meakins, M. W. Pemberton, R. N. Young, "Hydroxy-Steroids. Part XI. The Preparation and Infrared Spectra of Vicinal Cholestanediols", *J. Chem. Soc. C* **1968**, 2674–2682.

[16] F. A. J. Singelenberg, J. H. V. D. Maas, "Fourier Transform—Infrared Study of Hydrogen-Bonding between an OH-Donor and a Vicinal Oxygen Acceptor", *J. Mol. Struct.* **1990**, *240*, 213–223.

[17] K. Yamamoto, Y. Nakao, Y. Kyogoku, H. Sugeta, "Vibrational Circular Dichroism in Hydrogen Bond Systems: Part III. Vibrational Circular Dichroism of the OH Stretching Vibrations of 1,2-Diols and β-Methoxyalcohols", *J. Mol. Struct.* **1991**, *242*, 75–86.

[18] R. M. Parrish, L. A. Burns, D. G. A. Smith, A. C. Simmonett, A. E. DePrince, E. G. Hohenstein, U. Bozkaya, A. Y. Sokolov, R. Di Remigio, R. M. Richard, J. F. Gonthier, A. M. James, H. R. McAlexander, A. Kumar, M. Saitow, X. Wang, B. P. Pritchard, P. Verma, H. F. Schaefer, K. Patkowski, R. A. King, E. F. Valeev, F. A. Evangelista, J. M. Turney, T. D. Crawford, C. D. Sherrill, "Psi4 1.1: An Open-Source Electronic Structure Program Emphasizing Automation, Advanced Libraries, and Interoperability", *J. Chem. Theory Comput.* **2017**, *13*, 3185–3197.

[19] T. M. Parker, L. A. Burns, R. M. Parrish, A. G. Ryno, C. D. Sherrill, "Levels of Symmetry Adapted Perturbation Theory (SAPT). I. Efficiency and Performance for Interaction Energies", *J. Chem. Phys.* **2014**, *140*, 094106.

[20] M. J. Frisch, G. W. Trucks, H. B. Schlegel, G. E. Scuseria, M. A. Robb, J. R. Cheeseman, G. Scalmani, V. Barone, B. Mennucci, G. A. Petersson, H. Nakatsuji, M. Caricato, X. Li, H. P. Hratchian, A. F. Izmaylov, J. Bloino, G. Zheng, J. L. Sonnenberg, M. Hada, M. Ehara, K. Toyota, R. Fukuda, J. Hasegawa, M. Ishida, T. Nakajima, Y. Honda, O. Kitao, H. Nakai, T. Vreven, J. A. Montgomery, Jr., J. E. Peralta, F. Ogliaro, M. Bearpark, J. J. Heyd, E. Brothers, K. N. Kudin, V. N. Staroverov, R. Kobayashi, J. Normand, K. Raghavachari, A. Rendell, J. C. Burant, S. S. Iyengar, J. Tomasi, M. Cossi, N. Rega, J. M. Millam, M. Klene, J. E. Knox, J. B. Cross, V. Bakken, C. Adamo, J. Jaramillo, R. Gomperts, R. E. Stratmann, O. Yazyev, A. J. Austin, R. Cammi, C. Pomelli, J. W. Ochterski, R. L. Martin, K. Morokuma, V. G. Zakrzewski, G. A. Voth, P. Salvador, J. J. Dannenberg, S. Dapprich, A. D. Daniels, Ö. Farkas, J. B. Foresman, J. V. Ortiz, J. Cioslowski, D. J. Fox, Gaussian 09 Revision E.01, Gaussian Inc. Wallingford CT **2009**.